J Solid State Electrochem (2009) 13:1147–1155
DOI 10.1007/s10008-008-0656-6

REVIEW

Hydrogen evolution reaction on Sn, In, and Sn–In alloys in carboxylic acids

Hossnia S. Mohran · Abdel-Rahman El-Sayed · Hany M. Abd El-Lateef

Received: 12 April 2008 / Revised: 3 August 2008 / Accepted: 18 August 2008 / Published online: 9 September 2008

Abstract The cathodic behavior of tin, indium, and tin–indium alloys in 0.5-M solutions of oxalic, malic, and citric acids has been investigated using potentiodynamic techniques at temperature range of 30–60 °C. The results showed that the corrosion rate (I_{corr}) is higher at lower indium percent (0.5% In) and starts to decrease gradually as increase of the In percent up to 5% In (although it is still higher than that of pure tin and lower than that of indium at 5% In) in all examined acids. The positive shift in corrosion potential with simultaneous increase in corrosion rate can be explained on the basis of the depolarizing action of β-$InSn_4$ phase compared with pure tin. The negative shift in the corrosion potential with much higher corrosion rate in case of alloys IV and V (10% and 20% In, respectively) can be ascribed to the formation of γ-In_3Sn phase which leads to the increase in the anodic to cathodic area ratio. The corrosion of the two investigated metals and their alloys is affected by the formation of soluble complex species with organic acid anions. The aggressiveness of the studied metals and their alloys decreases in the following order of the organic acids employed oxalic > malic > citric acid. The observed activation energy values support that the tested electrodes exhibit higher corrosion rates in oxalic acid solution than the corresponding values in the other investigated acids. X-ray diffraction and scanning electron microscopy photographs elucidated the types of phases formed in the prepared alloys. The presence of a definite amount of indium in tin alloy improves the hardness.

H. S. Mohran (✉) · A.-R. El-Sayed · H. M. Abd El-Lateef
Chemistry Department, Faculty of Science Sohag,
Sohag University,
82524, Sohag, Egypt
e-mail: hossniamohran@yahoo.com

Keywords Potentiodynamic · Alloys · Hydrogen evolution · Corrosion

Introduction

Tin is widely used for the protection of cans. Successful packing of food in the cans is greatly dependent upon the unique ability of tin to protect steel from corrosion. The resistance of tinned plate towards corrosion is related to the interrelationship of characteristics of the can and the product packed therein. Tin may behave as a cathode or anode with respect to steel, depending upon the nature of the corrosion medium [1]. Indium is used for coating high-speed bearings, transistors, rectifiers, thermistors, and photoconductors. Tin–indium alloys are often used as the last step in a sequential soldering operation and for soldering to metallization on temperature-sensitive components. In order to prevent pollution of the environment with lead, the use of lead will be limited in many parts of the world in the near future. In the electronics industry, efforts are now being made to develop a usable lead-free solder, and several tin-based alloys have already been proposed. The goal in the development of lead-free solder is to produce alloys with nearly the same properties as those of lead solder, and most research up to now has focused on melting point and physical strengths of alloys [2]. The physical strength is related to metallography, which depends on thermal history and time. However, there is little information on the corrosion properties of base alloys for lead-free solder [3]. Despite numerous publications on tin in carboxylic acid solutions [4–7], there is not any information in the literature on In and Sn–In alloys particularly in solutions of carboxylic acids. Munoz and Bessone [8] studied cathodic behavior of In in

aqueous sodium chloride solutions. They found that the behavior of In in chloride solutions depends on the ratio of surface concentration Cl^- to OH^- in the potential region studied. Under stagnant condition, the hydrogen evolution reaction may generate an important change in the concentration of surface OH^-, leading to a Cl^- to OH^- ratio quite different from that present in the bulk solution. Thus, if Cl^- adsorption prevails, the formation of a surface salt film is possible.

The aim of this paper is to get more knowledge about the electrochemical trends of the Sn–In-based alloys at various compositions. In this sense, the cathodic behavior of the recent Sn–In alloys, prepared in our laboratory, is compared with that of pure metals (Sn and In) in the solutions of carboxylic acids at different temperatures.

Experimental

Materials and solutions

Oxalic, malic, and citric acids of 0.5-M solution (analytical grade) were prepared by dissolving the appropriate weight in doubly distilled water. Tin and indium of high purity (99.999%; Johnson Matthey Chemicals Ltd.) were used to prepare both Sn and In and Sn–In alloys as disk electrodes (A=0.196 cm^2) in a Gallenkamp muffle furnace using evacuated closed silica tubes at 700 °C for 24 h. The melts were shaken every 6 h to ensure the homogeneity of melting alloys and finally the melts were quenched in ice as previously discussed [9]. Five Sn–In alloys were prepared with the composition as following:

Alloy	I	II	III	IV	V
In (mass %)	0.5	2	5	10	20

The prepared alloys were analyzed using X-ray photoelectron spectroscopy. For each alloy, the percentage of Sn and In was found in accord with the percentage of mixing Sn and In. The microhardness of tin and prepared Sn–In alloys was measured using a Leiz Wetzlar Microhardness tester with a vickers diamond pyramid indicator; a load of 50 g was used, and the microhardness was expressed in kilograms per square millimeter.

Surface characterization

X-ray diffraction of the prepared alloys was carried out using a diffractometer with an iron filter and copper radiation was used with an accelerating voltage of 30 kV and a filament current of 20 mA. The morphology of the surface of Sn, In, and Sn–In alloys was examined using scanning electron microscope (SEM; JEOL, model 5300).

Electrochemical measurements

The measurements were performed on planar disk electrode embedded in an Araldite holder. Prior to each measurement, the electrodes were polished with sequacious grades of emery paper, degreased in pure ethanol, and washed in running bidistilled water before being inserted in the polarization cell. The reference electrode was a saturated calomel electrode (SCE) to which all potentials are referred. The cell description is given elsewhere [1]. To remove any surface contamination and air-formed oxide, the electrode was kept at −1,500 mV (SCE) for 5 min in the solution under test and disconnected shaken free of adsorbed hydrogen bubbles and then cathodic polarization was recorded by means of Potentiostat/Galvanostatic (EG&G Model 273) connected with a personal computer (IBM Model 30). The potential was altered automatically from higher negative potential −750 mV up to open-circuit potential ($E_{o.c.p}$) and at a scan rate of 1 mV/s using software version 342C supplied from EG&G Princeton Applied Research.

Each experiment was performed with freshly prepared solution and clean set of electrodes. Measurements were conducted at 30, 40, 50, and 60±0.5 °C for each investigated acid solution. For this purpose, ultra thermostat model Frigiter 6000 382(SELECTA) was used.

Results and discussion

Mechanical properties and composition of Sn, In, and Sn–In alloys

Microhardness measurements

The data in Fig. 1 reveal that the microhardness increases with increasing In percent in the alloy up to 5% In, while a relative decrease of the microhardness is observed at 10% In in the alloy. On the other hand, the microhardness starts to increase again at 20% In and reaches approximately the same value of 5% In. The increase in microhardness can be explained on the basis that the addition of In to Sn can result in the formation of intermetallic compounds in the solid state [9]. Intermetallic compounds are generally brittle and hard [10]. The bonding character of Sn–In alloys can be assumed as to be mainly metallic. Accordingly, the existence of indium in certain percent in Sn alloy would lead to the improvement of mechanical properties of Sn. It is clear from Fig. 1 that the relative decrease in microhardness at 10% In (11.30±0.15 HV) is observed. This behavior may be ascribed to the fact that, at this concentration of In, there would be little transformation of γ-$InSn_4$ into β-In_3Sn phase which represents an inversion point in some physical

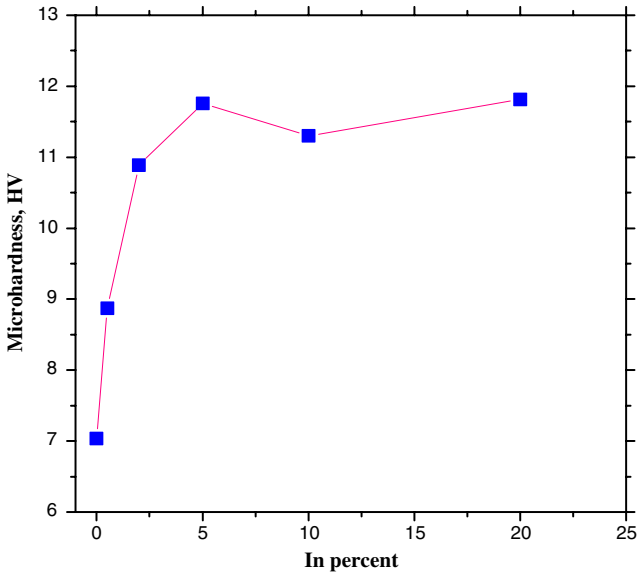

Fig. 1 Variation of microhardness with indium percent in the specimen

properties. This interpretation is supported by Koyama et al. [11]. They suggested that the Sn–In alloys containing 8.0–9.5% In undergo a phase transformation between the β-Sn and the (β-In_3Sn) simple hexagonal according to X-ray diffraction data.

X-ray diffraction

The data given in Fig. 2 show X-ray diffraction of Sn–In alloys **III** (5% Indium) prepared by the usual melt-quench technique which consists of a Sn–In intermetallic structure with the same ratio of the mixture. However, some separated Sn and In in their elemental phases can exist together with Sn–In matrix in the alloy. It is found that two phases form Sn–In alloys. X-ray diffraction shows that Sn forms γ-phase (γ-$InSn_4$- Tetragonal) with indium until 5% percent (alloys **I**, **II**, and **III**) and β-phase (β-In_3Sn-Hexagonal) with more than 5% indium (alloys **IV** and **V**).

SEM photographs

SEM photographs were performed in order to follow the change in microstructure as a result of alloying the Sn and In elements under the formerly described conditions. Typical SEM micrographs are shown in Fig. 3a–d for samples of (a) Sn, (b) In, and (c) alloy(**V**) (20% indium).

Figure 3a illustrates the microstructure and surface morphology of the nominal monophase Sn sample at magnification of ×2,000. The surface has a longitudinal flake-like shape. The micrograph illustrates a pure metallic phase with no valuable existence of the amorphous phase although the sample was prepared under the same conditions of the former samples. This may cause confusion because the sample was obeyed to quenching process during the preparation procedures. But the quenching condition may be not sufficient for amorphous phase formation of the pure Sn.

The micrograph of the monophase sample of In shown in Fig. 3b at magnification of ×2,000 illustrates a dense structure with very smooth surface. This indicates the quality of the sample preparation. The weak appearance of the dark regions on the surface indicates the poor existence of the amorphous phase which reflects the domination of the metallic one.

Figure 3c,d shows the photomicrograph corresponding to the nominal composition 80% Sn (alloy **V)** at magnifications of ×2,000 and ×3,500**.** The sample morphology was found to be influenced profoundly with the Sn intercalation. Dark-colored phase spreads widely on the surface and become competitive with the light-colored phase dissemination. The existence of these two phases in such form shown on the micrograph is clear evidence that the InSn crystallites are embedded in an amorphous matrix. On the other hand, the irregularity in their distribution may

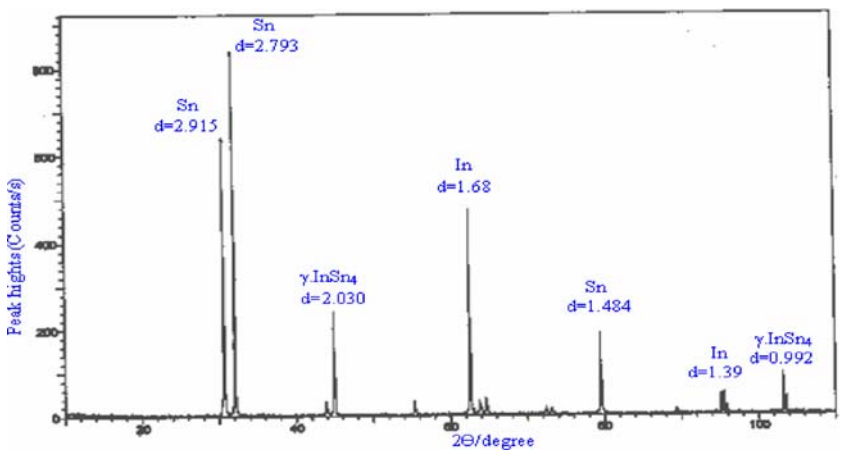

Fig. 2 X-ray diffraction patterns for alloy III (5% indium)

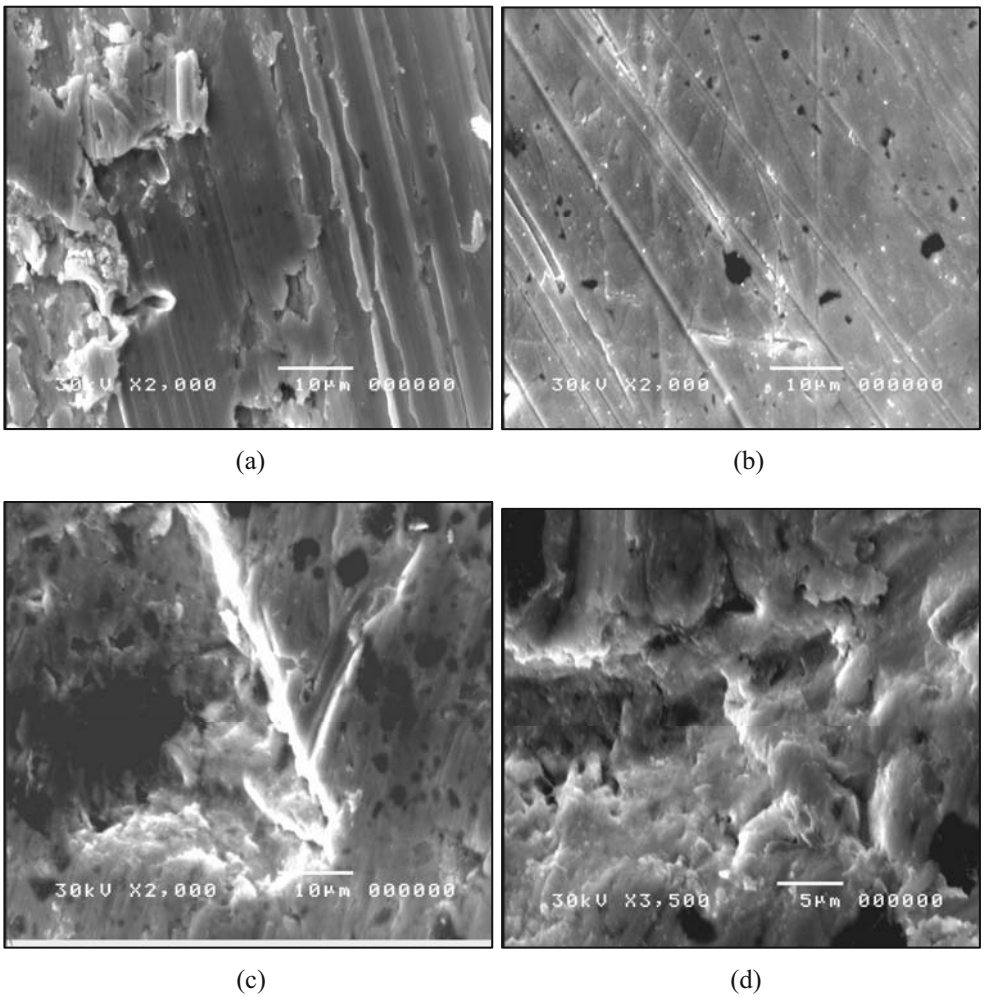

Fig. 3 SEM photographs of the surface of **a** Sn at magnification ×2,000, **b** In at magnification ×2,000, **c** alloy (**V**) at magnification ×2,000 and **d** alloy (**V**) at magnification ×3,500

emphasize the heterogeneity of the prepared sample. Besides, the overlapping between the dark and light grains at their boundaries reflects the connectivity strength between the amorphous and metallic phases which in turn refers to the hardness of the investigated sample.

Cathodic polarization behavior in the pure carboxylic acid solutions

Mechanism of hydrogen evolution reaction

It was found that the cathodic polarization obeys Tafel equation. The data given in Figs. 7, 8, 9, and 10 for the parameters of hydrogen evolution reaction including E_{corr} and I_{corr} values of pure tin, indium, and tin–indium alloys in 0.5-M solutions of oxalic, malic, and citric acid indicate that the cathodic Tafel slope (b_c) amounts to a value of 140±25 mV per decade at 30 °C. The corresponding value for the transfer coefficient (α) lies between 0.36 and 0.58. The observed values indicate that the processes correspond to a simple discharge mechanism for hydrogen evolution reaction.

Values of the cathodic Tafel slope greater than $2.303 \times 2 RT/F$ may be regarded as anomalous. It has been observed that the presence of surface film, presumably semiconducting, increases the values of the cathodic Tafel slope before surface activation [12–14].

The slight increase of cathodic Tafel slope (b_c) relative to the theoretical value with the corresponding relative values of α can be ascribed to the effect of adsorption of organic acid molecules at the electrode surface. This adsorption leads to the formation of an oriented dipole layer on the electrode surface, resulting in a distortion of the symmetry of potential distribution at the phase boundary (0.36–0.58). Values of cathodic Tafel slope for hydrogen evolution reaction on tin, nickel, and Sn–Ni alloy in acetic acid solution obtained by Kuhn et al. [15] were found to range from 168 to 180 mV.

Lower value of b_c in case of alloy **V** (20% indium) in citric acid solutions than those obtained in oxalic and malic acid solutions is observed. This behavior is attributed to the fact that the film formed on the alloy surface in citric acid is relatively less thick than the corresponding one formed in the other investigated carboxylic acids solutions. Figures 4,

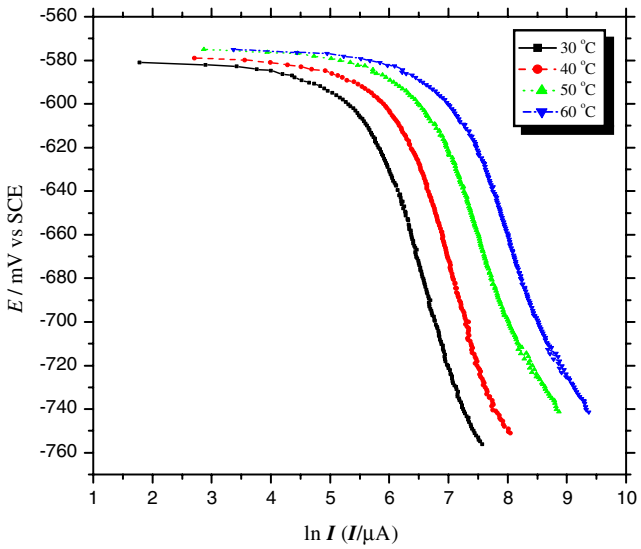

Fig. 4 Potentiodynamic cathodic polarization curves for alloy (III) in 0.5-M oxalic acid solutions

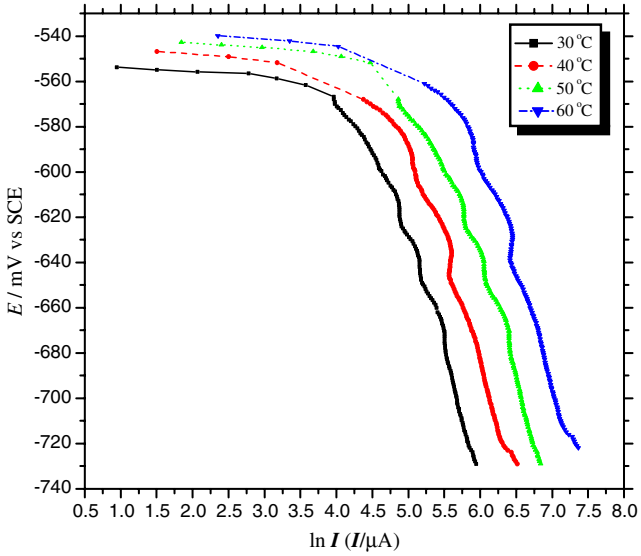

Fig. 6 Potentiodynamic cathodic polarization curves for alloy (III) in 0.5-M citric acid solutions

5, and 6 show the potentiodynamic cathodic polarization curves for alloy III in 0.5-M solutions of oxalic, malic, and citric acids, respectively.

Corrosion behavior and the effect of the acids nature

The corrosion potential (E_{corr}) and corrosion rate (I_{corr}) for tin, indium, and their investigated alloys in 0.5-M solutions of oxalic, malic, and citric acid at different temperatures are given in Figs. 7, 8, 9, and 10. The data showed that E_{corr} shifts to a more positive direction with an increase in In percent in the alloy up to 5% In compared with E_{corr} of pure tin at 30 °C. However, it shifts to a more negative direction at higher In percent than that in the alloy (at 10% and 20% In) in oxalic acid solution at the same temperature. This positive shift is associated with a pronounced increase in the corrosion rate of alloys compared with both pure tin and indium. However, it is observed that the corrosion rate is higher at lower In percent in the alloy **I** (0.5% indium) and starts to decrease gradually with an increase in In percent up to 5% In (although it is still higher than that of pure tin and lower than that of indium at 5% In).

The positive shift in corrosion potential with simultaneous increase in corrosion rate can be ascribed to the

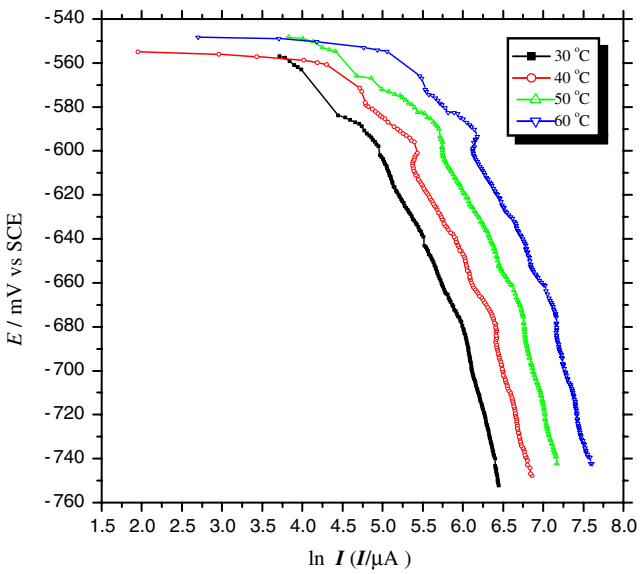

Fig. 5 Potentiodynamic cathodic polarization curves for alloy (III) in 0.5-M malic acid solutions

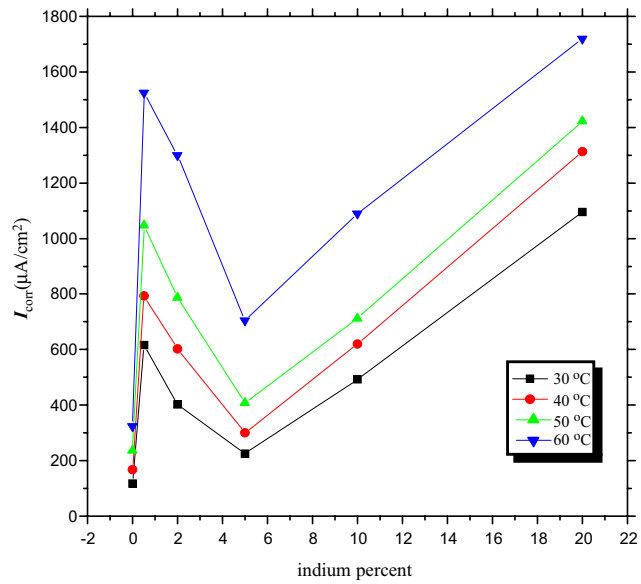

Fig. 7 Variation of I_{corr} of Sn with increase in indium percentage in the specimen in 0.5-M oxalic acid solution at different temperature

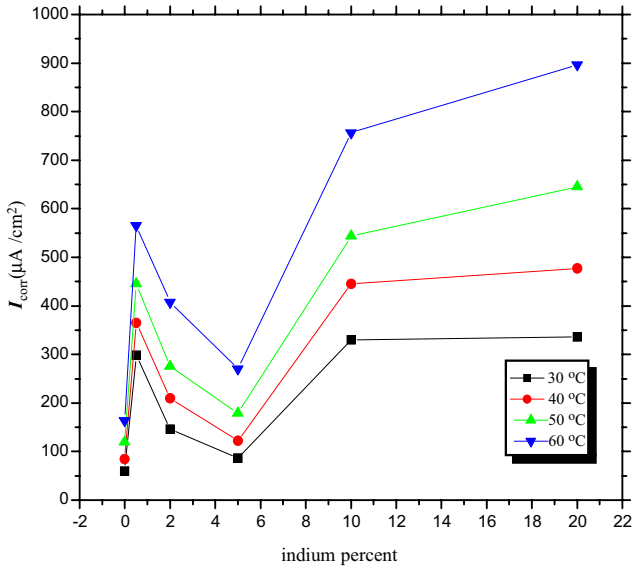

Fig. 8 Variation of I_{corr} of Sn with increase in indium percentage in the specimen in 0.5-M malic acid solution at different temperature

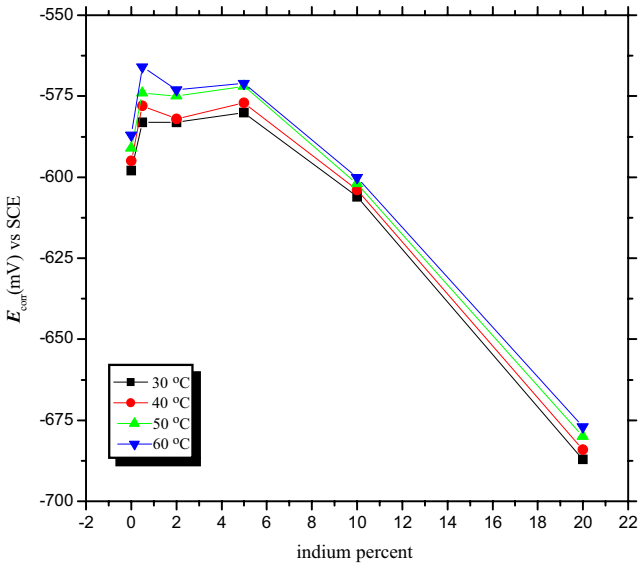

Fig. 10 Variation of E_{corr} of Sn with increase in indium percentage in the specimen in 0.5-M oxalic acid solution at different temperature

depolarizing action of the $InSn_4$ phase (which is recorded using X-ray diffraction) in the alloy. Since hydrogen overpotential on the particles of $InSn_4$ may be lower than that of pure tin [16], it is concluded that $InSn_4$ phase present as a separated phase or in pearlitic structure acts as cathodic sites in the presence of tin. However, the depolarizing action is higher at lower In percent (0.5% indium). Therefore, it is assumed that the presence of indium as a minor alloying element increases the active sites' density at the surface and consequently increases rate of complex formation with the carboxylic acid anions adsorbed at the surface. The results obtained by Thanh et al. [17] indicated that the alloying constituents in Al substrates

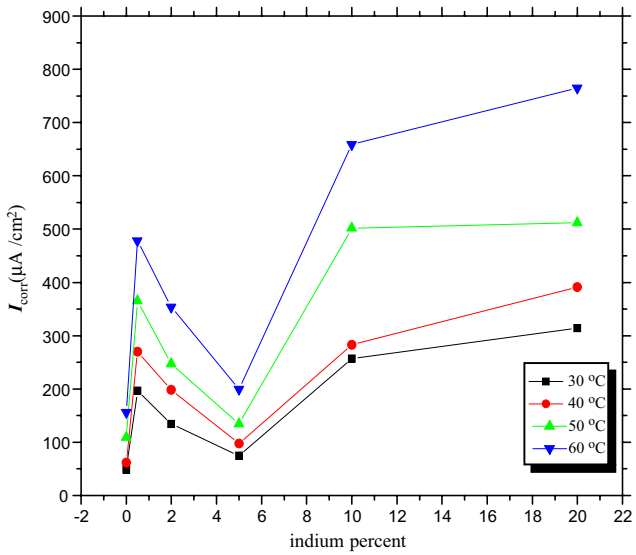

Fig. 9 Variation of I_{corr} of Sn with increase in indium percentage in the specimen in 0.5-M citric acid solution at different temperature

play an important role in the formation of active sites. The positive shift of corrosion potential in case of alloy **I** indicate the rate of dissolution of oxide film is high [18]. This agrees with the values obtained for corrosion rate (I_{corr}) using the cathodic polarization measurements (Fig. 7). On the other hand, it is observed that the depolarizing action decreases with increasing In percent up to 5% indium. This may be due to eutectoide composition formation particularly at 5% indium in the alloy. X-ray diffraction confirmed that γ-$InSn_4$ phase is formed in the alloy up to 5% indium percent.

The negative shift in E_{corr} of alloys **IV** and **V** relative to that observed of pure tin, with sharp increase in corrosion rate, may be ascribed to change in the microstructure from $InSn_4$ phase (up to 5% indium) to In_3Sn phase (at 10% and 20% indium). X-ray diffraction confirmed that γ-phase (γ-$InSn_4$-Tetragonal) is formed in the alloys (**I**, **II**, and **III**), while β-phase (β-In_3Sn- Hexagonal) is formed in the alloys (**IV** and **V**). Koyama et al. [11] reported that the Sn–In alloys containing 8.0–9.5% In undergo a phase transformation between the β-Sn and the (β-In_3Sn) simple hexagonal structure with varying temperature. Accordingly, the change of trend at higher In percent (alloys **IV** and **V**) may be attributed to the difference in the amount and distribution of indium containing phases (intermetallic compound) on the alloy surface. Therefore, an increase in the anode to cathode area ratio may occur. On the other hand, the inflection points in Fig. 4 may be related to the adsorption of oxalate anions on the electrode surface near the open-circuit potential [1].

Values of the steady-state corrosion potential (E_{corr}) and corrosion rate (I_{corr}) for pure tin, indium, and the investigated Sn–In alloys in 0.5-M solution of malic acid showed

that the corrosion potential (E_{corr}) shifts to a more negative direction with an increase in In percent in the alloy. On the other hand, the results obtained for corrosion rate (I_{corr}) of all the investigated electrodes in malic acid solution exhibited similar trends to those encountered with oxalic acid solution. The corrosion rate is much higher in alloy **I** (lower indium percent) and starts to decrease gradually with an increase in In percent in the alloy up to 5%. However, the corrosion rates increase again at higher In percent more than 5% (10% and 20% indium in the alloy).

The higher corrosion rate of alloy **I** (0.5% indium) compared with those of pure tin and alloys **II** and **III** can be attributed to the presence of a minor element from indium in the Sn matrix. This in turn facilitates the hydrogen evolution reaction on the alloy surface [19], while an increase of In percent in the alloy up to 5% leads to relative decrease of corrosion rate which attains its maximum value (lower value) with alloy **III** (5% indium). This fact can be due to the higher formation of $InSn_4$ phase in the alloy surface leading to less heterogeneous surface [20].

As mentioned before, the negative shift in the corrosion potential with simultaneous increase in corrosion rate in the case of alloys **IV** and **V** (10% and 20% indium) can be ascribed to the formation of γ-In_3Sn phase, leading to an increase of the anodic to cathodic area ratio. Munoz et al. [21] found that the presence of In as solid solution promotes the corrosion of Al–In alloy in NaCl solution.

The results obtained in citric acid solution show that the corrosion behavior of Sn, In, and examined five alloys is similar to their behavior in malic acid solution. However, the presence of In does not affect the corrosion potential of alloys **I** and **II** compared with its effect on E_{corr} of pure tin. But E_{corr} shifts gradually to a more negative potential with the increase of In percent, starting from alloy **III** (5% indium), and attains its maximum (more negative shift) with alloy **V** (20% indium) compared with pure tin.

A comparison of corrosion rate for all investigated electrodes in the examined three acids is carried out under the same conditions. It is observed that the aggressiveness decreases in the following order:

oxalic acid>malic >citric

It is of interest to find that this order follows the same sequence of the stability constants. The values of the acidity constants (first ionization constant in the case of dicarboxylic and tricarboxylic acids) follow the order: oxalic ($K_1=5.6\times10^{-2}$) > malic ($K_1=9.1\times10^{-4}$) > citric ($K_1=7.4\times10^{-4}$) [22]. It is found that, for the same acid concentration, the higher corrosion rate corresponds to the large value of dissociation constant [6]. Seruga and Hasenay [23] found that the corrosion rate of Al in oxalic is higher than that in malic and citric acid solutions. Skine and Ksenoo [24] found that the corrosion rate of steel is higher in formic acid than in acetic acid (at the same acid concentration) and the difference in corrosion rate was attributed to the fact that the dissociation constant of formic acid is higher than that of acetic acid.

Higher corrosion rate are obtained in oxalic acid solution compared to those in malic and citric acid solutions. This can be ascribed mainly to the higher acidity of oxalic acid solution than those of malic and citric acid solutions at the same acid concentration and to the higher stability of M-oxalate complex species compared to those of malate and citrate. Similar results were obtained by Abd El Rehim et al. [1] for the corrosion of tin in carboxylic acid solutions. They found that the highest corrosion rate of tin is observed in oxalic acid solution.

Effect of alloying with indium on the corrosion behavior of tin

Comparison of corrosion rate obtained for all investigated Sn–In alloys in the examined carboxylic acid solutions at different temperatures (30–60 °C) indicates that there is a large difference between them. The results exhibit that the corrosion rate is much higher in the case of alloy **V** (20% indium) than that in other investigated alloys. The corrosion rate follows the order:

$$\begin{aligned}\text{Alloy } \mathbf{V}\ (20\%\ \text{indium}) &> \mathbf{IV}\ (10\%\ \text{indium})\\ &> \text{alloy}\mathbf{I}\ (0.05\%\ \text{indium})\\ &> \text{alloy}\ \mathbf{II}\ (2\%\ \text{indium})\\ &> \text{alloy}\ \mathbf{III}\ (5\%\ \text{indium}).\end{aligned}$$

This is consistent with the previous assumption that two phases for Sn–In alloys are formed. X-ray diffraction confirmed that Sn forms γ-phase (γ-InSn4- Tetragonal) with indium percent up to 5% indium, while it forms β-phase (β-In3Sn-Hexagonal) with more than 5% indium.

Figure 11 represents polarization curves for alloy III in 0.5-M solution of oxalic acid at different temperature. It can be seen that the temperature affected both cathodic and anodic branches of the polarization curves towards higher current densities. Similar curves are obtained in 0.5-M solutions of malic and citric acids for all investigated electrodes under the same conditions. By comparison, between I_{corr} values obtained from cathodic polarization curves and I_{corr} obtained from extrapolation of anodic and cathodic curves Fig. 11, we find that both have a similar trend. Similar behavior was observed in both malic and citric acid solutions.

These results are similar to those obtained by Che et al. [25] and Lee et al. [26]. Mendelssohn and Shiffman [27] found that the alloys with less than 5% indium show the maximum in the intermediate state thermal resistively in case of pure metals. The presence of β-phase (hexagonal) in the alloys **(IV** and **V**) leads to higher corrosion than that

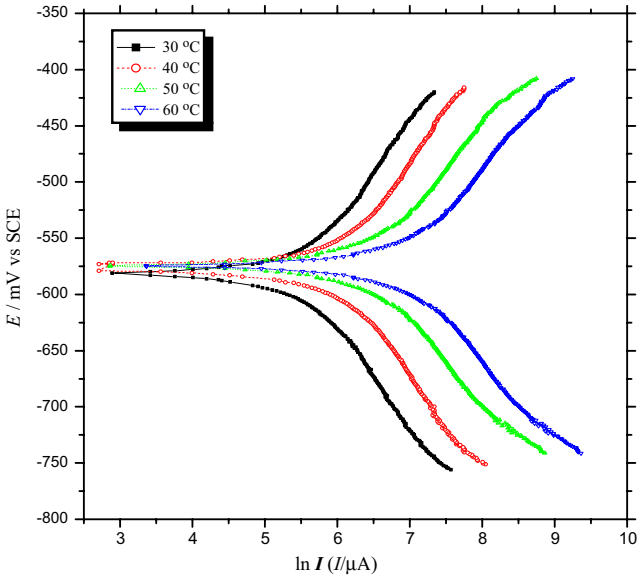

Fig. 11 Polarization curves for alloy (III) in 0.5-M oxalic acid solution at a scan rate of 1 mV s^{-1}

of γ-phase (tetragonal) present in alloys (**I**, **II**, and **III**). This behavior may be attributed to the greater surface area in the case of hexagonal structure than that of tetragonal structure. Accordingly, it has been found that the corrosion resistance of the examined electrodes decreases (except in the case of alloy **III** with corrosion rate lower than that of indium) in the following order:

Sn>In>Sn−In alloys.

The higher activity of Sn–In alloy is interpreted on the basis of the autocatalytic attack by indium. The initial dissolution of Sn–In alloy leads to the increase of the concentration of In^{3+} ions in the electrolyte; then, the redeposition of In at active sites on the electrode surface occurs, leading to the enhanced activity**.** Abedin and Endres [28] found that Al–In alloy exhibits the highest negative breakdown potential in 0.6 M NaCl and the corrosion resistance of the examined electrodes decreases in the following order:

Al>Al−Ga−In>Al−In.

Effect of In percent on the activation energy of the corrosion process of tin and tin–indium alloys

Table 1 shows the values of the apparent activation energy (E_a) for tin, indium, and their alloys in oxalic, malic, and citric acids. These values are determined from the slope of Arrhenius plots (log I_{corr} against $1/T$ plots as shown in Fig. 12 applying the equation:

$$I_{corr} = A \exp(-E_a/RT) \quad (1)$$

Where I_{corr} is the corrosion rate, A is the frequency factor, E_a the activation energy, and T absolute temperature. It can

Table 1 Apparent activation energy in kilojoule per mole of tin, indium, and Sn–In alloys in 0.5-M oxalic, malic, and citric acids solutions

Metal and alloys	Oxalic acid E_a (kJ/mol)	Malic acid E_a (kJ/mol)	Citric acid E_a (kJ/mol)
Tin	14.4	15.21	15.52
Indium	12.82	13.53	13.8
Alloy I	10.90	11.80	12.10
Alloy II	11.50	12.30	13.00
Alloy III	13.62	13.88	14.50
Alloy IV	9.70	9.90	11.39
Alloy V	8.45	9.75	10.72

be observed that the values of E_a for pure tin in citric and malic acid solutions are approximately the same (15.1± 0.3 kJ mol^{-1}) and slightly different in oxalic acid (14.1 kJ mol^{-1}). These values are in agreement with those obtained by Abd El Rehim et al. [1] for the corrosion of tin in citric acid solution. A similar trend is observed for pure tin in the investigated acid solutions. Although values of E_a for alloys **IV** and **V** are appreciably lower than those for pure tin, indium, and the other three alloys, they are approximately the same irrespective of the nature of the carboxylic acid. The lower values of E_a in the case of alloys **IV** and **V** run parallel with its higher corrosion rate of these alloys. This may be ascribed to the higher active sites and/or an increase anodic to cathodic area ratio. The data exhibited that the value of activation energy E_a for tin, indium, and their alloys increases in the following order:

citric >malic>oxalic acid

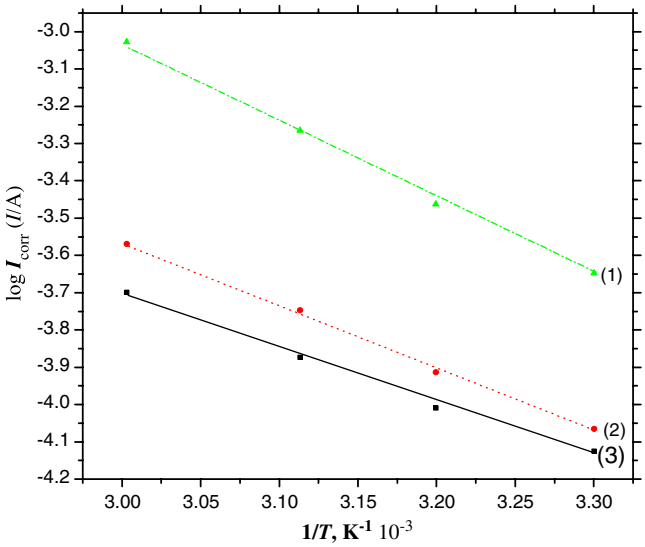

Fig. 12 Arrhenius plots for alloy III corrosion in 0.5-M (*1*) oxalic acid, (*2*) malic acid, and (*3*) citric acid solutions

Higher values of E_a in citric acid solution compared with those obtained in the other examined acids may be ascribed to strong adsorbability of the acid molecules on all investigated electrodes. Therefore, the increased adsorption of citric acid molecules decreases the active cathodic sites and consequently increases the standard heat of activation of hydrogen evolution reaction. El-Sayed [29] assumed that the adsorption occurs on the higher energy sites.

The currents at (−100 mV vs. O.C.P) are plotted vs. $1/T$ to estimate the apparent activation energy values of hydrogen evolution reaction alone. The observed values have been found almost equal to the corresponding values estimated at the corrosion potential. This issue suggests that the hydrogen evolution reaction would be the rate-limiting process.

Conclusions

1- X-ray diffraction and SEM photographs show that $InSn_4$ phase is found in Sn–In alloys having up to 5% In, while In_3Sn phase is found in alloy containing more than 5% In.
2- Addition of In to Sn increases the microhardness; accordingly, the existence of In in a certain percent in Sn alloy leads to the improvement of mechanical properties of Sn.
3- Corrosion rate is higher at lower In percent (0.5% In) and starts to decrease gradually with an increase of In percent in the alloy up to 5% in all investigated acids. This behavior can be attributed to the presence of In (at 0.5% In) as minor alloying element which increases the active sites at the surface and consequently increases the rate of complete formation with the carboxylic acid anions. The results suggest that alloy III (5% In) has lower corrosion rate compared with the other investigated alloys; this trend may be due to the formation of eutectoid composition, leading to less heterogeneous surface.
4- A comparison between corrosion rate of all investigated electrodes in oxalic, malic, and citric acids indicates that the order of decreasing their aggressiveness is as follows:

   oxalic>malic>citric

5- The results of activation energy (E_a) exhibit that all investigated electrodes have lower values of E_a in oxalic acid compared to those obtained in the other examined acids. This behavior supports that the corrosion rate of the examined metals and their alloys is higher in oxalic acid than the other investigated acids.
6- Generally, the greater activity of Sn–In alloys is due to the autocatalytic attack by indium. The initial dissolution of Sn–In alloy leads to an increase in the concentration of In^{3+} ions in the electrolyte. The redeposition of In (particularly at cathodic polarization) at active sites on the electrode surface occurs, leading to the enhanced activity.

References

1. Abd El Rehim SS, Hassan HH, Mohamed NF (2004) Corros Sci 46:1071. doi:10.1016/S0010-938X(03)00134-3
2. Taguchi M, Hirasawa T, Wada K (2006) J Power Sources 158:1456. doi:10.1016/j.jpowsour.2005.10.079
3. Dezhi L, Paul PC, Changqing L (2008) Corros Sci 50:995. doi:10.1016/j.corsci.2007.11.025
4. El-Sherbini EEF, Moussa SO, Abd El Rehim SS, Hamdy E (2007) J Appl Electrochem 37:533. doi:10.1007/s10800-005-9084-9
5. Abdel Rehim SS, Sayyah SM, El Deeb MM (2003) Mater Chem Phys 80:393. doi:10.1016/S0254-0584(03)00128-7
6. Abd El Rehim SS, Zaky AM, Mohamed NF (2006) J Alloy Comp 424:88. doi:10.1016/j.jallcom.2005.12.080
7. El-Sayed A, Abd El-Rehim SS, Mansour H (1991) Monatsh Chem 122:1019. doi:10.1007/BF00811110
8. Munoz AG, Bessone JB (1998) Electrochim Acta 43:2033. doi:10.1016/S0013-4686(97)10119-0
9. El-Sayed A, Shaker AM, Gad El-Kareem H (2003) Bull Chem Soc Jpn 76:1527. doi:10.1246/bcsj.76.1527
10. Kim HS, Lee KH, Shin MC (1998) Scr Mater 38:1549. doi:10.1016/S1359-6462(98)00071-2
11. Koyama Y, Nittono O, Suzuki H (1985) Scr Metall 18:715. doi:10.1016/0036-9748(84)90326-0
12. Kazuhisa ABB, Tomohiro U, Masahiro S (2004) J Electroanal Chem 567:1. doi:10.1016/j.jelechem.2003.11.057
13. Kunze J (1967) Corros Sci 7:273. doi:10.1016/0010-938X(67)80047-7
14. Hogyared T, Earl WB (1967) J Electrochem Soc 114:694. doi:10.1149/1.2426708
15. Kuhn AT, Neufeld P, Young K (1985) J Appl Electrochem 15:471. doi:10.1007/BF00616004
16. Cleary HJ, Greene ND (1967) Corros Sci 7:821. doi:10.1016/S0010-938X(67)80115-X
17. Thanh PT, Akiyama A, Saji T (1982) Electrochim Acta 27:847. doi:10.1016/0013-4686(82)80206-5
18. Dipuola A, Di Quarto F (1977) Electrochim Acta 22:63. doi:10.1016/0013-4686(77)85055-X
19. El Shayeb HA, Abd El Wahab FM, Zein El Abedin S (2001) Corros Sci 43:655. doi:10.1016/S0010-938X(00)00101-3
20. Abdul Azim AA, Sanad SH (1973) Corros Sci 13:869. doi:10.1016/S0010-938X(73)80069-1
21. Munoz AG, Saidman SB, Bessone JB (2002) Corros Sci 44:2171. doi:10.1016/S0010-938X(02)00042-2
22. Lurie J (1975) Handbook of analytical chemistry. Mir, Moscow
23. Seruga M, Hasenay D (2001) J Appl Electrochem 31:961. doi:10.1023/A:1017556323508
24. Sekine I, Senoo K (1984) Corros Sci 24:439. doi:10.1016/0010-938X(84)90069-6
25. Che S, Yanar C, Schwartz AJ, Massalski TB, Laughlin DE (2005) International Conference on Solid–Solid Phase 22
26. Lee JG, Mori H, Yasuda H (2005) Phys Rev B 65:132106. doi:10.1103/PhysRevB.65.132106
27. Mendelssohn K, Shiffman CA (1960) Proc R Soc Lond A Math Phys Sci 255:199. doi:10.1098/rspa.1960.0062
28. Abedin SZ, Endres F (2005) Passivation of metals and semiconductors and properties of thin oxide layers. In: 9th International Symposium Paris France, vol. 27, p 633
29. El-Sayed A (1997) J Appl Electrochem 27(2):193. doi:10.1023/A:1018456008267